Tb nanocrystalline array assembled directly from alloy melt

Y. T. Wang
Institute of Physics, Chinese Academy of Sciences, Beijing 100080, People's Republic of China
and College of Math and Physics, Chongqing University, Chongqing 400044, People's Republic of China

X. K. Xi, Y. K. Fang, D. Q. Zhao, M. X. Pan, B. S. Han, and W. H. Wang[a)]
Institute of Physics, Chinese Academy of Sciences, Beijing 100080, People's Republic of China

W. L. Wang
College of Math and Physics, Chongqing University, Chongqing 400044, People's Republic of China

(Received 26 July 2004; accepted 1 November 2004)

A two-dimensional (2D) thin film composed of Tb nanocrystals with uniform orientations is fabricated directly from $Tb_{65}Fe_{25}Al_{10}$ alloy melt upon quenching. The Tb nanocrystals with vertical height of 15–30 nm and lateral width of 10–20 nm are assembled in the nanocrystalline array on an amorphous substrate. The formation mechanism for the aligned Tb nanocrystals is discussed. The single-step formation method may provide a new and flexible alternative to fabricate nanostructured films or arrays used for submicron devices. © *2004 American Institute of Physics*.
[DOI: 10.1063/1.1836863]

Self-assembled nanocrystalline film or array with uniform orientations is highly desirable and their availability is closely associated with the various emerging nanotechnologies, such as submicron magnetoelectronics devices,[1,2] ultrahigh density magnetic recordings.[3,4] As a result, a variety of fabrication methods have been developed, for example, microwave plasma-enhanced chemical vapor deposition, sol-gel techniques, electrodeposition, etc.[5] Recently intensive effort has been carried out to synthesize bulk nanocrystalline composites from metallic glasses or alloy melts by using solid state processing[6] or liquid quenching methods.[7] Experimentally, the rare-earth (RE, RE=Nd, Pr, Y, and Sm) nanocrystals have been observed randomly embedded in RE–Fe–Al glass matrix under the conditions far from thermodynamic equilibrium,[8–10] which opens a gap to assemble nanostructured film directly from the alloy melt. The microstructure and physical properties of such nanostructured films or arrays should have intrinsic characteristics, and will be of significance to expand current understanding of nanostructure fabrication.

In this work, we present a way of direct assembling two-dimensional (2D) fine nanostructured film from the $Tb_{65}Fe_{25}Al_{10}$ alloy melt upon quenching. Terbium is one of the largest magnetostriction materials in low temperature, the magetostriction constant λ is up to 8700 ppm, which is almost two orders of magnitude higher than other uniaxial materials (e.g., bcc-Fe, fcc-Ni, hcp-Co, Gd, etc.).[11] This allows the dimension of the Tb nanocrystal to be easily tuned in a scale according to the external magnetic field. Therefore, the Tb nanocrystalline array with uniform orientations may have potential applications for submicron actuators, transducers, and storage devices. The present method may eliminate the cumbersome traditional process and is potentially a flexible way to fabricate nanostructured film or array.

Master alloy with a nominal composition of $Tb_{65}Fe_{25}Al_{10}$ was prepared by arc melting Tb, Fe, and Al with a purity of 99.9% in a titanium-gettered argon atmosphere. The ingots were remelted several times to ensure the homogeneity of the samples. The ribbons with a thickness of 20–100 μm were prepared by a single roller melt-spinning apparatus at the wheel surface velocities of 5–25 m/s in argon atmosphere. The structure of the melt-spun ribbons was characterized by x-ray diffraction (XRD) in a MAC M03 XHF diffractometer with Cu $K\alpha$ radiation. Thermal analysis was performed using a Perkin-Elmer DSC-7 differential scanning calorimeter under a continuous argon flow at a heating rate of 20 K/min. Calorimeter was calibrated for temperature and energy with high purity indium and zinc. The topography of the ribbon was studied by using atomic force microscope (AFM) at a Digital Instruments NanoScope IIIa D-3000 AFM.

Figure 1 shows the XRD patterns of the $Tb_{65}Fe_{25}Al_{10}$ melt-spun ribbons at different wheel velocities. All the surfaces of the as-spun ribbons appear smooth and lustrous. For the ribbon spun at 25 m/s, the XRD pattern shows a broad maximum peak followed by a lesser intensity broad peak indicating almost amorphous phase. When the spin velocity decreases to 10 m/s, a broadening crystalline peak is superimposed on the XRD curve due to the formation of fine nanocrystals,[7] and the ribbon has a mixed microstructure of nanocrystalline and amorphous phases. The crystalline peaks

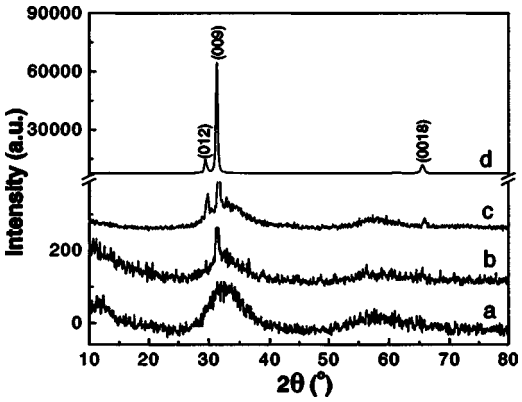

FIG. 1. XRD patterns of the $Tb_{65}Fe_{25}Al_{10}$ ribbons at different wheel velocities: (a) 25 m/s, free surface; (b) 10 m/s, free surface; (c) 5 m/s, powder pattern; (d) 5 m/s, free surface.

[a)]Electronic mail: whw@aphy.iphy.ac.cn

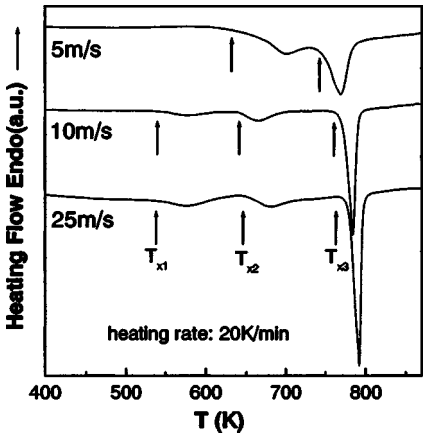

FIG. 2. DSC curves of the $Tb_{65}Fe_{25}Al_{10}$ ribbons at different wheel velocities. The heating rate is 20 K/min.

match exactly with that of Tb phase as shown in Fig. 1. While at wheel velocity of 5 m/s, only Tb phase and no amorphous phase can be detected on the free surface of the ribbon [see Fig. 1(d)]. Closer examination of the XRD pattern in Fig. 1(d), one can find the much stronger Tb (009) peak (the others are rather weak, even cannot be detected), which strongly suggests that the hexagonal Tb phase has a strong texture with *c*-axis predominantly perpendicular to the ribbon plane.[8] According to the Scherrer formula[12] and neglecting possible strain contributions, the average height of the particle along *c*-axis is estimated to be about 28 nm, which is consistent with the following AFM observation. However, when the ribbon spun at 5 m/s is milled into powder, both the amorphous phase and crystalline Tb can be seen in the XRD curve [see Fig. 1(c)], and the intensity of the Tb peak is sharply decreased, which further confirms that Tb nanocrystal particles standing on the free surface of the amorphous ribbon have uniform orientations.

Figure 2 presents the DSC curves for the $Tb_{65}Fe_{25}Al_{10}$ melt-spun ribbons, which also exhibit the microstructural evolution of the ribbon upon wheel velocities. At the 25 m/s, the ribbon undergoes three steps of crystallization corresponding to three distinct exothermic peaks: two broad peaks ($T_{x1}=542$ K, $T_{x2}=651$ K) appear before a sharp peak with onset at 780 K. No obvious endothermic event due to a glass transition is visible, in agreement with previous results of RE-based metallic glass;[8] the sharp exothermic peak at 780 K is due to massive crystallization. There is no apparent difference in T_{x2} or T_{x3} for the ribbons quenched with different wheel velocities. In contrast, the broad peak at T_{x1} diminishes with the precipitation of Tb nanocrystalline, and disappears completely when a large numbers of Tb nanocrystals form at wheel velocity of 5 m/s, indicating that T_{x1} is the starting precipitation temperature of the Tb nanocrystal.

Figure 3 shows the atomic force microscope (AFM) images ($1\mu m\times 1\mu m$) of the free surface of melt-spun $Tb_{65}Fe_{25}Al_{10}$ ribbons with different wheel velocities. The AFM investigations were carried out directly on the free surface of the ribbons, which reveal the microscopic morphology of the samples. For the ribbon spun at velocity of 25 m/s, no obvious nanocrystals are observed on the free surface in nanoscale [see Fig. 3(a)], which is in good agreement with that the amorphous state of the sample. However, when the wheel velocity decreases to 5 m/s, the surface roughness increases sharply from 0.3 to 6.5 nm, a large number of nanocrystals are found to precipitate on the ribbon surface [see Fig. 3(b)]. The observations further confirm the XRD and DSC results. The Tb nanoparticles exhibit randomly distribution over the whole surface; from the statistical results got from a large number of section analyses, the vertical height and lateral width are mainly within the range of 15–30 and 10–20 nm, receptively (When measuring small nanoparticle, the AFM has a lateral magnification effect due to its tip size, so the lateral width is measured by SEM.[13]

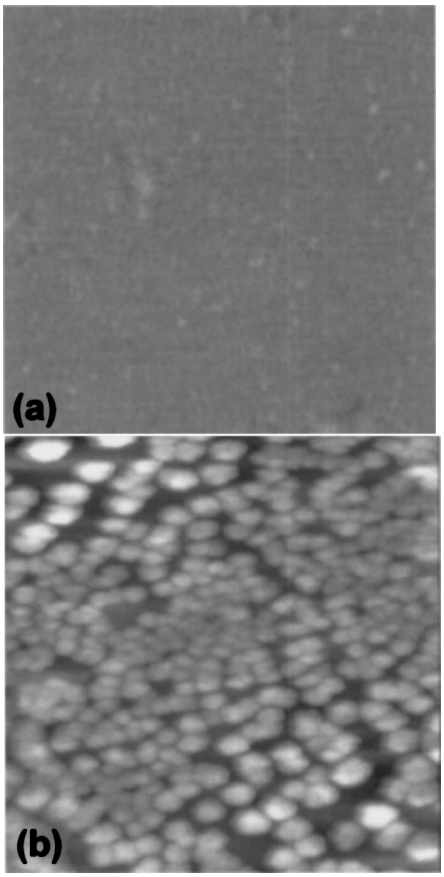

FIG. 3. (Color online): AFM images ($1\ \mu m\times 1\ \mu m$) of the $Tb_{65}Fe_{25}Al_{10}$ ribbons: (a) 25 m/s, free surface; (b) 5 m/s, free surface.

To give more details, the AFM image with a larger scale ($5\mu m\times 5\mu m$) is shown in Fig. 4. The nanocrystalline has

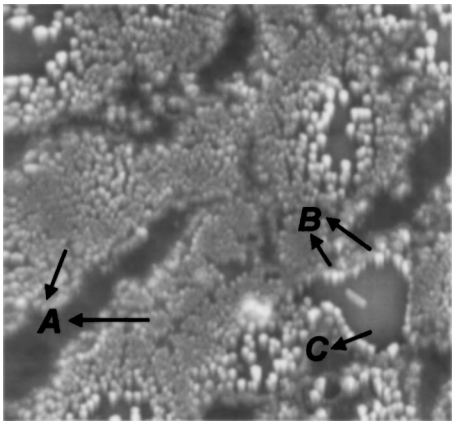

FIG. 4. (Color online): AFM image ($5\ \mu m\times 5\ \mu m$) of the $Tb_{65}Fe_{25}Al_{10}$ ribbon melt spun at 5 m/s. (a) the nanostructured film composed of Tb nanocrystallines; (b) the hexagonal Tb nanocrystallines with uniform orientations; (c) the exposed bottom amorphous matrix.

formed a compact and two-dimensional (2D) film in most areas (indicated by marker *A*). From the edge of the film, it can be clearly seen that the aligned columelliform nanocrystallines were grown vertically on the surface of the ribbon (marked by *B*). These freestanding nanocrystallines have been discerned to be the hexagonal Tb phase with *c*-axis predominantly perpendicular to the ribbon plane by XRD measurements, resulting in the very strong Tb (009) XRD peak. The region marked by *C* shows the exposed amorphous matrix, which is smooth and has been detected by XRD when the ribbon is milled into powder.

The mechanism responsible for the nanostructured film formation is speculated as follows. A larger negative heat of mixing of the constituents, ΔH_{mix} is necessary to stabilize metallic glass. However, the ΔH_{mix} between the two main components (Tb and Fe) is less negative (-2 kJ/mol) and hence liquid is to be less stable, consequently leading to clustering between like atoms.[8,14] The precipitation of RE particles is found to be a common phenomenon for RE–Fe–Al glass-forming (RE=Nd, Pr, Y, Sm).[8,9,15] At the nucleation stage, Tb nanocrystals have random orientations, but the nanocrystal growth is strongly influenced by the diffusion field and mutual impingement.[8,16] On the free surface of ribbons, those standing on the surface almost vertically have more stronger diffusion field and lesser diffusion field impingement, which may result from the steep temperature gradient in the direction perpendicular to the ribbon plane, so these Tb nuclei preferably grow up normal to the ribbon plane, and finally assemble the nanostructured array with uniform orientations.

In summary, we have presented a fabrication of nanostructured film directly from alloy melt. The two-dimensional thin film composed of aligned Tb nanocrytals with uniform orientations is assembled directly from the $Tb_{65}Fe_{25}Al_{10}$ alloy upon quenching. Terbium has excellent magnetostriction properties in low temperature, so the array assembled by Tb nanocrystalline could have potential for applications. The present way eliminates the cumbersome traditional process and is potentially a new and flexible approach to fabricate nanostructured film used for submicron devices.

The authors are grateful for the financial support of the National Natural Science Foundation of China (Grant No. 50321101) and experimental assistance of B. Zhang and Y. X. Wei.

[1] J. L. Simonds, Phys. Today **48**, 26 (1995).
[2] G. A. Prinz, Science **282**, 1660 (1998).
[3] S. Y. Chou, P. R. Krauss, and P. B. Fischer, Science **272**, 85 (1996).
[4] M. H. Kryder, W. Messner, and L. R. Carley, J. Appl. Phys. **79**, 4485 (1996).
[5] Carl C. Koch, *Nanostructured Materials: Processing, Properties and Potential Applications* (Noyes, New York, 2002).
[6] W. H. Wang, D. W. He, D. Q. Zhao, and Y. S. Yao, Appl. Phys. Lett. **75**, 2770 (1999); W. H. Wang, R. J. Wang, and D. Q. Zhao, J. Mater. Res. **17**, 1385 (2002); K. Lu, Mater. Sci. Eng., R. **16**, 161 (1996); J. Q. Su, T. W. Nelson, and C. J. Sterling, J. Mater. Res. **18**, 1757 (2003).
[7] J. M. Li, Appl. Phys. Lett. **84**, 347 (2004); W. H. Guo and H. W. Kui, Acta Mater. **48**, 2117 (2000).
[8] Z. G. Sun, W. Löser, J. Eckert, K.-H. Müller, and L. Schultz, Appl. Phys. Lett. **80**, 772 (2002); Z. G. Sun, W. Löser, J. Eckert, K.-H. Müller, L. Schultz, T. Zhu, and Z. H. Cheng, J. Appl. Phys. **93**, 6930 (2003).
[9] Y. Li, S. C. Ng, Z. P. Lu, Y. P. Peng, and K. Lu, Philos. Mag. Lett. **78**, 213 (1998).
[10] J. J. Kim, Y. Choi, S. Suresh, and A. S. Argon, Science **295**, 654 (2002).
[11] R. C. O'Handley, *Modern Magnetic Materials: Principles and Applications* (John Wiley, New York, 2000).
[12] B. D. Cullity, *Elements of X-Ray Diffraction*, 2nd ed. (Addison-Wesley, London, 1978), p. 101.
[13] Y. J. Chen, W. Y. Chenung, I. H. Wilson, N. He, S. P. Wong, J. B. Xu, H. Sang, and G. Ni, Appl. Phys. Lett. **72**, 2472 (1998).
[14] B. S. Murty and K. Hono, Appl. Phys. Lett. **84**, 1674 (2004).
[15] W. H. Wang, D. Q. Zhao, and H. Y. Bai, J. Phys.: Condens. Matter **16**, 3719 (2004).
[16] D. R. Allen, J. C. Foley, and J. H. Perepezko, Acta Mater. **46**, 431 (1998).